A coupled SPH-DEM model for the simulation of abrasive water-jet impacting solid surface

***Ran Yu, †Xiangwei Dong, and Zengliang Li**

College of Mechanical and Electronic Engineering, China University of Petroleum (East China), China

*Presenting author: yr_liquid@163.com
†Corresponding author: dongxiangweiupc@163.com

Abstract

Numerical model of the smoothed particle hydrodynamics method (SPH, a meshfree numerical method), has been approved its great advantages in fluid–particle-solid coupling problems with free surfaces, such as abrasive water-jet (AWJ) impacting process. However, the fully resolved SPH method needs a large amount of computation because of the requirement for fine resolution, which limits its application in practical problems. Coupling of the discrete element method (DEM) and SPH may be a more effective way to achieve the goal. In this study, a coupled SPH-DEM unresolved model is proposed for simulation of AWJ impact. The water-jet and the solid are discretized with a series of SPH particles, and each abrasive is modeled by a DEM particle. Different smoothing lengths are used for SPH-SPH particles and SPH-DEM particles, resulting in a multiple linked-list search method for neighborhood searching. The SPH and DEM particles are coupled through the so-called local averaging technique, in which the interaction forces between the two phases are related to the local porosity. Compared with the fully resolved SPH model, the new coupled model is more efficient, and is suitable for fluid-particle-solid simulation. The process of the single abrasive water-jet impact on the solid is simulated to verify the applicability of the model. The cases of single particle settlement is also involved. Results show that the proposed model can accurately capture the motion of particles in complex fluid flows, and has less computation time cost, which could be useful in the applications of AWJ machining and complex fluid-particle flow with free surfaces.

Keywords: Smoothed particle hydrodynamics; Discrete element method; Abrasive water-jet; Fluid–particle-solid interaction; Free surface flow

1 Introduction

The issue of the fluid–particle flows impacting solid surface is a common concern in several engineering fields, such as coastal, fluvial, and transportation engineering [1]. Abrasive water-jet (AWJ) is a typical fluid–particle flow, which has been widely used in various industries, such as cutting, mining and drilling [2,3]. It involves the interactions between fluid, abrasives, and the solid in free surface flows. Adjustment of various parameters makes the experimental study of AWJ time-consuming and expensive [4]. So the numerical simulation of AWJ impact process can be a valuable complement to the experiments to reveal the fundamental behaviors and predict the solid erosion performance [5].

As both Lagrangian methods, the smoothed particle hydrodynamics method (SPH) has more advantages than the finite element method (FEM) in dealing with large displacement and large deformation problems. In our previous research [6, 7, 8], a fully resolved SPH model for AWJ simulation was proposed and improved. Both fluid, abrasives and solid material were modeled by SPH particles. The water-jet was modeled as a continuous fluid flow, the solid was modeled as elastic–plastic material, and the abrasives were treated as rigid bodies. The model had the advantages of simple concept and strong robustness. The erosion process of the metallic surface by AWJ impact was reproduced. However, the large amount of computation is one of the disadvantages of the previous SPH model. In this study, we propose a coupled SPH-DEM model for AWJ simulation to improve the computational efficiency. Each abrasive is simplified to a single DEM particle, instead of a series of SPH particles. The locally averaged density algorithm based on the local porosity is adopted to simulate the movement of abrasives in water-jet flow. The new proposed model not only realize the detailed interaction among the water-jet, abrasives and solid, but also reduces the number of neighborhood SPH particle pairs, which reduces the computation cost.

The remainder of this study is organized as follows. In Sec.2 and Sec.3, the basic theory of coupled SPH-DEM algorithm is presented, and the modeling process is described. In Sec.4, two cases of single particle settlement and single abrasive water-jet impact are presented to prove the validity of the coupled model. In Sec.5, the conclusions of the study are summarized.

2 Formulations for SPH model (Fluid and solid phase)

This section summarizes some fundamental parts of SPH model based on the local averaging technique.

2.1 Basic theory of SPH

In SPH model, materials in the computational domain are discretized by a set of particles, which carry field variables and material properties, such as velocity, density, stress, etc [9]. When a SPH particle is within another SPH particle's support domain **Ω**, those two particles interact with each other and move according to the governing equations, as shown in Fig.1. Each particle moves according to its own acceleration. Therefore, this method is not limited by the mesh factors and is suitable for large deformation simulation [10].

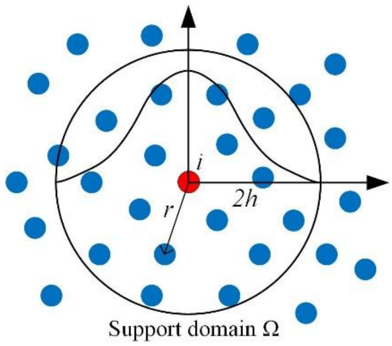

Figure 1. Kernel approximation in SPH method

There are two main steps for the SPH model establishment. The first step is the integral representation of field functions (kernel approximation). The value of the field function $f(\boldsymbol{x})$ can be approximated as the integral representation of $\boldsymbol{x}'$ in the support domain Ω of $\boldsymbol{x}$ [11]. The second step is the particle approximation, which discretize the continuous integral function into the sum of the finite particles located in the support domain $\mathbf{\Omega}$ of $\boldsymbol{x}$. As show in follows:

$$\langle f(\boldsymbol{x}_i)\rangle = \sum_{j=1}^{N}\frac{m_j}{\rho_j} f(\boldsymbol{x}_j)\cdot W(\boldsymbol{x}_i-\boldsymbol{x}_j,h)\,, \tag{1}$$

$$\left\langle \frac{\partial f(\boldsymbol{x}_i)}{\partial \boldsymbol{x}}\right\rangle = \sum_{j=1}^{N}\frac{m_j}{\rho_j} f(\boldsymbol{x}_j)\cdot \frac{\partial W_{ij}}{\partial \boldsymbol{x}_i}\,, \tag{2}$$

where $\boldsymbol{x}_i$ and $\boldsymbol{x}_j$ in Eq. (1) and Eq. (2) are the position vectors of particle i and j, respectively. Particle j represents the SPH particle which is located in the support domain $\mathbf{\Omega}$ of the particle i. m_j and ρ_j are the mass and the density of the particle j, respectively. N is the total number of the particles within the support domain $\mathbf{\Omega}$ of particle i. The kernel gradient $\frac{\partial W_{ij}}{\partial \boldsymbol{x}_i}$ can be expressed as $\frac{\partial W_{ij}}{\partial \boldsymbol{x}_i} = \frac{\boldsymbol{x}_i - \boldsymbol{x}_i}{r_{ij}}\frac{\partial W_{ij}}{\partial r_{ij}} = \frac{\boldsymbol{x}_{ij}}{r_{ij}}\frac{\partial W_{ij}}{\partial r_{ij}}$, where r_{ij} is the distance between particle i and j.

There are many available smoothing functions for SPH model. The cubic spline function, which was proposed by Monaghan and Lattanzio [12], is used in this study:

$$W(\boldsymbol{x}_i-\boldsymbol{x}_j,h) = W_{ij} = a_d \times \begin{cases} \frac{2}{3} - q^2 + \frac{1}{2}q^3, & 0 \le q < 1 \\ \frac{1}{6}(2-q)^3, & 1 \le q < 2 \\ 0, & q \ge 2 \end{cases}, \tag{3}$$

where q is the relative distance between the particle i and j (q=r_{ij}/h), a_d is the normalization constant which is expressed as a_d =15/(7πh^2) for the two-dimensional simulation.

2.2 Local averaging technique for SPH model (Fluid phase)

In this paper, the fluid and the solid phase are treated as continuous media. To calculate the coupling force between SPH and DEM particles, a local averaging technique is introduced. The concept was established by Anderson and Jackson [13] to deal with the momentum exchange and balance between different phases. For ease of reading, the SPH particles are labeled as particle a and b while the DEM particles are labeled as particle i and j. For the fluid SPH particle a, the locally averaged fluid density $\bar{\rho}_a$ is shown as:

$$\bar{\rho}_a = \varepsilon_a \rho_f\,, \tag{4}$$

where ε_a is the local porosity of the fluid particle a, and ρ_f is the actual fluid density. The local porosity ε_a depends on the volume fraction of nearby DEM particles smoothed by the kernel function, as shown in follows [14]:

$$\varepsilon_a = 1 - \sum_j W_{aj}(h_c)V_j\,, \tag{5}$$

where $W_{aj}(h_c)$ is the SPH kernel function and h_c is the coupling smoothing length between SPH and DEM particles. h_c should be larger than the diameter of DEM particle but small enough to capture local feature of the porosity field. V_j is the volume of DEM particle.

For fluid SPH particles, the conservation equations of mass and momentum based on local averaging technique are expressed as:

$$\frac{\mathrm{d}\overline{\rho}_a}{\mathrm{d}t}=\overline{\rho}_a\sum_{b=1}^{N}\frac{m_b}{\overline{\rho}_b}(\boldsymbol{v}_a^{\beta}-\boldsymbol{v}_b^{\beta})\cdot\frac{\partial W_{ab}}{\partial \boldsymbol{x}_a^{\beta}}, \tag{6}$$

$$\frac{\mathrm{d}\boldsymbol{v}_a^{\alpha}}{\mathrm{d}t}=\sum_{b=1}^{N}m_b\left[-\left(\frac{P_a}{\overline{\rho}_a^{2}}+\frac{P_b}{\overline{\rho}_b^{2}}\right)\delta^{\alpha\beta}+\Pi_{ab}^{visc}-\pi_{ab}^{art}\delta^{\alpha\beta}\right]\cdot\frac{\partial W_{ab}}{\partial \boldsymbol{x}_a^{\beta}}+\boldsymbol{f}_a^{\alpha}, \tag{7}$$

where α and β are the Cartesian coordinates x and y, and t represents the time. $\delta^{\alpha\beta}$ is the Kronecker tensor (if $\alpha=\beta$, $\delta^{\alpha\beta}=1$, otherwise, $\delta^{\alpha\beta}=0$). $\boldsymbol{f}_a^{\alpha}$ is the external force of the particle a, such as gravity or coupling forces. The first term in Eq.(7) is the pressure term. The second term (Π_{ab}^{visc}) is the dissipative force, which is treated as the viscosity force in Newtonian fluids [15]. The third term (π_{ab}^{art})is the artificial viscosity term, which is proposed by Monaghan to reduce unphysical spurious oscillations and improve the numerical stability.

For fluid SPH particles, the pressure P is a function of the actual density ρ, which is computed by the eqution of state (EOS). A Mie-Grüneisen form of the EOS for fluid particles is shown as [16]:

$$P=\frac{\rho_0 c_0^2\eta\left[1+\left(1-\frac{\Gamma_0}{2}\right)\eta-\frac{a}{2}\eta^2\right]}{\left[1-(S_1-1)\eta-S_2\frac{\eta^2}{\eta+1}-S_3\frac{\eta^2}{(\eta+1)^2}\right]^2}+(\Gamma_0+a\eta)e, \tag{8}$$

where $\eta=\rho/\rho_0$, ρ_0 is the reference density and ρ is the actual density. e is the internal energy per unit of mass. Table 1 lists the EOS parameters of fluid phase.

Table 1. EOS parameters for fluid phase[16]

Parameters	Value
Reference density	ρ_0=1000kg/m^3
Velocity of sound	c_0=1480m/s
Grüneisen gamma	Γ_0=0.5
Volume correction coefficient	a=0
Coefficient	S_1=2.56
Coefficient	S_2=1.98
Coefficient	S_3=1.23

2.3 Formulations for SPH model (Solid phase)

In this study, the solid phase is modeled as a elastic–plastic material to investigate the erosion process by AWJ impact. Similar to Section 2.2, the conservation equations for solid SPH particles are written as:

$$\frac{\mathrm{d}\rho_a}{\mathrm{d}t}=\rho_a\sum_{b=1}^{N}\frac{m_b}{\rho_b}(\boldsymbol{v}_a^{\beta}-\boldsymbol{v}_b^{\beta})\cdot\frac{\partial W_{ab}}{\partial \boldsymbol{x}_a^{\beta}}, \tag{9}$$

$$\frac{\mathrm{d}\boldsymbol{v}_a^{\alpha}}{\mathrm{d}t}=\sum_{b=1}^{N}m_b\left[-\left(\frac{P_a}{\rho_a^{2}}+\frac{P_b}{\rho_b^{2}}\right)\delta^{\alpha\beta}+\frac{\tau_a^{\alpha\beta}+\tau_b^{\alpha\beta}}{\rho_a\rho_b}-\Pi_{ab}\delta^{\alpha\beta}\right]\cdot\frac{\partial W_{ab}}{\partial \boldsymbol{x}_a^{\beta}}+\boldsymbol{f}_a^{\alpha}, \tag{10}$$

where the second term in Eq.(10) is the shear force term. $\tau_a^{\alpha\beta}$ is the deviatoric stress of the particle a. $\boldsymbol{f}_a^{\alpha}$ is the external force, such as gravity or contact force with DEM particles.

In the elastic-plasticity mechanics, the deviatoric stress rate $\dot{\tau}_a^{\alpha\beta}$ is a function of the strain rate tensor $\varepsilon_a^{\alpha\beta}$ and the rotation rate tensor $R_a^{\alpha\beta}$. The incremental formulation with the Jaumann rate correction is shown as follows [11]:

$$\dot{\tau}_a^{\alpha\beta} = \frac{\mathrm{d}\tau_a^{\alpha\beta}}{\mathrm{d}t} = 2G\left(\varepsilon_a^{\alpha\beta} - \frac{1}{3}\delta^{\alpha\beta}\varepsilon_a^{\gamma\gamma}\right) + \tau_a^{\alpha\gamma}\cdot R_a^{\beta\gamma} + \tau_a^{\gamma\beta}\cdot R_a^{\alpha\gamma}, \tag{11}$$

where G is the shear modulus. $\varepsilon_a^{\alpha\beta}$ is the strain rate tensor and $R_a^{\alpha\beta}$ is the rotation rate tensor, respectively.

The Johnson–Cook constitutive model (J-C) is selected to descripe the plastic deformation of OFHC copper [17], which is numerically robust and easily implemented in the SPH formulations. The yield stress σ_y in J-C model is written as:

$$\sigma_y = \left[A + B\left(\varepsilon_{eff}^p\right)^N\right]\left[1 + C\ln\left(\frac{\dot{\varepsilon}_{eff}^p}{\dot{\varepsilon}_0}\right)\right], \tag{12}$$

where ε_{eff}^p is the equivalent plastic strain, $\dot{\varepsilon}_{eff}^p$ is the equivalent plastic strain rate, and $\dot{\varepsilon}_0$ is the reference strain rate. A, B, C and N are material dependent constants.

The oxygen-free high-thermal-conductivity (OFHC) copper is selected as the solid phase material. The Mie-Grüneisen EOS equation for OFHC copper is employed as [18]:

$$P = \frac{\rho_0 c_0^2 \eta\left[1 + \left(1 - \frac{\Gamma_0}{2}\right)\eta\right]}{\left[1 - (S_a - 1)\eta\right]^2} + \rho_0\Gamma_0 e, \tag{13}$$

where S_a is a linear Hugoniot slope coefficient, the EOS parameters for OFHC copper are shown in Table 2.

Table 2. EOS parameters for OFHC copper[18]

Parameters	Value
Reference density	ρ_0=8960kg/m^3
Velocity of sound	c_0=3940m/s
Grüneisen gamma	Γ_0=1.99
Linear Hugoniot slope coefficient	S_a=1.5

3 Formulations for DEM model (Abrasive phase) and phase coupling

DEM is a Lagrangian method proposed by Cundall [19] to study discontinuous mechanical efforts of rock by assemblies of discs (2D) or spheres (3D). Each abrasive is simplified to a single DEM particle. Contact forces occur when the particles overlap. The abrasive and fluid phase are coupled by local averaging algorithm based on porosity, which can be used to simulate the motion of abrasives in free surface flow.

3.1 DEM governing equations

The basic governing equations of DEM particles follow Newton's second law. In this study, the forces acting on the DEM particle i are listed as:

$$m_i\frac{d\boldsymbol{v}_i}{dt} = \sum_j \boldsymbol{F}_{ij}^c + \boldsymbol{F}_{fa} + \boldsymbol{F}_{sa}^c + m_i\boldsymbol{g}, \tag{14}$$

where m_i and $\boldsymbol{v}_i$ are the mass and velocity of DEM particle i, respectively. $\boldsymbol{F}_{ij}^{c}$ is the contact force for abrasive-abrasive interaction, and j represents other DEM particles contact with particle i. $\boldsymbol{F}_{fa}$ is the coupling force with fluid SPH particle, including drag force and buoyancy. $\boldsymbol{F}_{sa}^{c}$ is the contact force with solid SPH particles. For rotational motion, the angular acceleration of the DEM particle i is expressed as:

$$I_i \frac{d\boldsymbol{\omega}_i}{dt} = \sum_j \boldsymbol{T}_{ij} , \tag{15}$$

where I_i, $\boldsymbol{\omega}_i$, and $\boldsymbol{T}_{ij}$ are the moment of inertia, angular velocity, and torque of contact forces.

3.2 Contact force for abrasive-abrasive interaction

The details of contact force of DEM have been described in many literatures. To simulate interaction and rotation behavior among abrasives in water-jet flow, the soft-sphere contact force model is adopted in this study. The normal and tangential contact forces for abrasive-abrasive interaction are determined from the particle overlap by a spring-dashpot model [20]. The schematic illustration is shown in Fig.2.

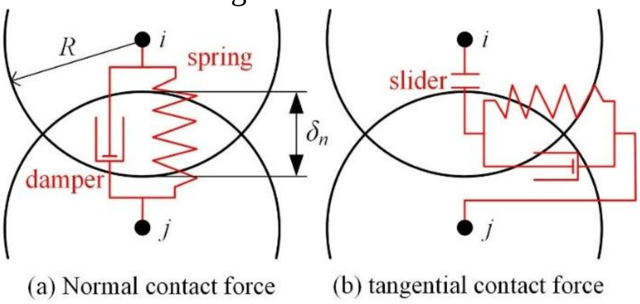

Figure 2. Schematic illustration of soft-sphere contact force model

The abrasives are treated as rigid bodies and the surface deformation is ignored. The soft-sphere model is suitable for numerical simulation of engineering problems. The contact force for the DEM particle i is the sum of normal and tangential forces, as follows:

$$\boldsymbol{F}_{ij}^{c} = \boldsymbol{F}_{ij}^{n} + \boldsymbol{F}_{ij}^{t} , \tag{16}$$

where the superscript n and t denote normal and tangential forces, respectively. The normal contact force is given by

$$\boldsymbol{F}_{ij}^{n} = -k_n \delta_n \boldsymbol{n}_{ij} - d_n \boldsymbol{v}_{ij}^{n} , \tag{17}$$

where k_n and d_n denote the normal stiffness and damping coefficient, respectively. δ_n is the normal overlap size between DEM particle i and j, as shown in Fig.2. $\boldsymbol{n}_{ij}$ is the unit normal vector, from i to j. $\boldsymbol{v}_{ij}^{n}$ is the normal relative velocity, which is determined by the relative velocity $\boldsymbol{v}_{ij}$, as shown in follows:

$$\boldsymbol{v}_{ij} = \boldsymbol{v}_i - \boldsymbol{v}_j + (R_i \boldsymbol{\omega}_i + R_j \boldsymbol{\omega}_j) \times \boldsymbol{n}_{ij} , \tag{18}$$

$$\boldsymbol{v}_{ij}^{n} = (\boldsymbol{v}_{ij} \cdot \boldsymbol{n}_{ij}) \boldsymbol{n}_{ij} , \tag{19}$$

where R and $\boldsymbol{\omega}$ are the radius and angular velocity of DEM particle, respectively.
Similar to normal force, the tangential contact force is written as:

$$\boldsymbol{F}_{ij}^{t}=-k_t\delta_t\boldsymbol{t}_{ij}-d_t\boldsymbol{v}_{ij}^{t}, \tag{20}$$

where k_t and d_t denote the tangential stiffness and damping coefficient, respectively. δ_t is the normal overlap size between DEM particle i and j. $\boldsymbol{t}_{ij}$ is the unit tangential vector, $\boldsymbol{t}_{ij}=\frac{\boldsymbol{v}_{ij}^{t}}{\left|\boldsymbol{v}_{ij}^{t}\right|}$. $\boldsymbol{v}_{ij}^{t}$ is the tangential relative velocity, $\boldsymbol{v}_{ij}^{t}=\boldsymbol{v}_{ij}-\boldsymbol{v}_{ij}^{n}$.

In addition, the maximum tangential force is limited by the slip condition:

$$\boldsymbol{F}_{ij\,\max}^{t}=\mu\left|\boldsymbol{F}_{ij}^{n}\right|\boldsymbol{t}_{ij}, \tag{21}$$

where μ is the friction coefficient at the contact.

The contact torque $\boldsymbol{T}_{ij}$ shown in Eq.(15) is determined by the tangential contact force $\boldsymbol{F}_{ij}^{t}$:

$$\boldsymbol{T}_{ij}=\boldsymbol{F}_{ij}^{t}\times(\boldsymbol{x}_i-\boldsymbol{x}_p), \tag{22}$$

where $\boldsymbol{x}_i$ is the center of gravity of the DEM particle i. $\boldsymbol{x}_p$ is the position of the contact point, which is on the line between particle i and j, and the distance from i is R.

3.3 Contact force for solid-abrasive interaction

The contact force $\boldsymbol{F}_{sa}^{c}$ for the solid-abrasive interaction is based on the penalty algorithm [21], as shown in Fig.3. The solid material is modeled as a elastic–plastic material (as shown in Sec.2.3), and the abrasives are modeled as rigid particles. When the distance between the solid SPH particle and the abrasive DEM particle is within the threshold (in this study, the threshold is set to $R+d_{ini}$, where R is the DEM particle's radius and d_{ini} is the initial spacing of two adjacent SPH particles), the contact force $\boldsymbol{F}_{sa}^{c}$ is generated. $\boldsymbol{F}_{sa}^{c}$ can be decomposed into the normal force $\boldsymbol{F}_{sa}^{n}$ and tangential force $\boldsymbol{F}_{sa}^{t}$.

$\boldsymbol{F}_{sa}^{n}$ and $\boldsymbol{F}_{sa}^{t}$ are expressed as:

$$\begin{cases}\boldsymbol{F}_{sa}^{n}=(1-\chi)\left[\dfrac{2m_a}{(\Delta t)^2}\left(R+d_{ini}-d_p\right)\right]\boldsymbol{n}_p\\ \boldsymbol{F}_{sa}^{t}=\dfrac{2m_a}{\Delta t}\left(\boldsymbol{v}_{pi}\cdot\boldsymbol{\tau}_p\right)\boldsymbol{\tau}_p\end{cases}, \tag{23}$$

where χ is the index of the penetration, if $\chi=0$ means no penetration is allowed. m_a is the mass of particle a, and Δt is the time step. $\boldsymbol{v}_{pi}=\boldsymbol{v}_p-\boldsymbol{v}_i$, where $\boldsymbol{v}_p$ is the velocity vector at point p.

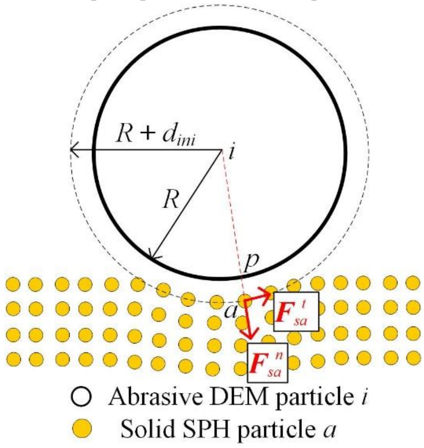

Figure 3. Illustration of solid-abrasive interaction

3.4 Coupling force for fluid-abrasive interaction

For the abrasive DEM particle *i*, coupling force $\boldsymbol{F}_{fa}$ due to fluid flow is modelled, which can be split into a hydrodynamic force and a drag force [22]:

$$\boldsymbol{F}_{fa} = V_i(-\nabla P + \nabla \cdot \tau)_i + \boldsymbol{f}_d(\varepsilon_i, \boldsymbol{u}_i), \tag{24}$$

where V_i is the volume of DEM particle *i*. For the hydrodynamic force, ∇P is the pressure gradient, and $\nabla \cdot \tau$ is the viscosity force. Drag force $\boldsymbol{f}_d$ depends on the local porosity ε_i and relative velocity $\boldsymbol{u}_i$ between fluid and abrasive.

The hydrodynamic force is evaluated at particle *i* using a Shepard corrected SPH interpolation, given as:

$$V_i(-\nabla P + \nabla \cdot \tau)_i = \frac{1}{\sum_a \frac{m_a}{\rho_a} W_{ia}(h_c)} \sum_a m_a \theta_a W_{ia}(h_c), \tag{25}$$

$$\theta_a = \sum_b m_b \left[-\left(\frac{P_a}{\bar{\rho}_a^2} + \frac{P_b}{\bar{\rho}_b^2} \right) + \Pi_{ab}^{visc} \right] \cdot \nabla_a W_{ab}(h), \tag{26}$$

where the subscript *a* is the fluid SPH particle nearby the DEM particle *i*. The subscript *b* is the fluid SPH particle nearby the particle *a*. *h* is the smoothing length among SPH particles, and h_c is the coupling smoothing length between SPH and DEM particles.

The drag force $\boldsymbol{f}_d$ is a function of local porosity ε_i and relative velocity $\boldsymbol{u}_i$. The local porosity ε_i at the position of DEM particle *i* is estimated by smoothing the nearby values of SPH particles: The expression for the drag force $\boldsymbol{f}_d$ is shown below:

$$\boldsymbol{f}_d = \frac{\beta_i}{1-\varepsilon_i} V_i \boldsymbol{u}_i, \tag{27}$$

where β_i is the interphase momentum transfer coefficient, which is given by:

$$\beta_i = \begin{cases} 150 \dfrac{(1-\varepsilon_i)^2}{\varepsilon_i} \dfrac{\mu_f}{d_i^2} + 1.75(1-\varepsilon_i) \dfrac{\rho_f}{d_i} |\boldsymbol{u}_i|, & \varepsilon_i \leqslant 0.8 \\ 0.75 C_d \dfrac{\varepsilon_i(1-\varepsilon_i)}{d_i} \rho_f |\boldsymbol{u}_i| \varepsilon_i^{-2.65}, & \varepsilon_i > 0.8 \end{cases}, \tag{28}$$

where μ_f, ρ_f are the viscosity, reference density of the fluid, respectively. C_d, d_i are the drag coefficient, diameter for DEM particle *i*, respectively.

The coupling force on fluid SPH particle *a* is calculated by a weighted average fluid-abrasive coupling force $\boldsymbol{F}_{fa}$ acting on the DEM particles nearby within the coupling length h_c. The contribution of each DEM particle to this average is scaled by the value of the SPH kernel function:

$$\boldsymbol{f}_a = -\frac{m_a}{\bar{\rho}_a} \sum_i \frac{1}{S_i} \boldsymbol{F}_{fa} W_{ai}(h_c), \tag{29}$$

where $\boldsymbol{F}_{fa}$ is the coupling force acting on DEM particles in Eq.(24). The scaling factor S_i is calculated to ensure that the force acting on the fluid particles is balanced with the force on the DEM particle, which is given by:

$$S_i = \sum_b \frac{m_b}{\rho_b} W_{bi}(h_c) , \tag{30}$$

where the subscript b is the fluid SPH particle nearby the DEM particle i within the coupling length h_c.

4 Validations of the coupled SPH-DEM model

According to the formulations presented above, the SPH-DEM 2D numerical model is implemented by a Fortran code in this study. In this section, two numerical cases are proposed to verify the coupled model correctly handle the interactions among different phases. Meanwhile, compared with the fully resolved SPH model [6~8], this model has the advantage of less computation and higher computational efficiency.

4.1 Case 1: single particle sedimentation

The first case simulates the process of a single particle sedimentation in a fluid domain by gravity. The results are compared with the data in Reference [23] to verify the coupled model can simulate the coupling force between DEM and SPH phases.

Computational domain of the single particle sedimentation is shown in Fig.4. The water area is 0.04×0.06m, and the initial height for the single DEM particle is 0.04m. The gravity acts in the negative Y direction. Other detailed parameters are listed in Table 3.

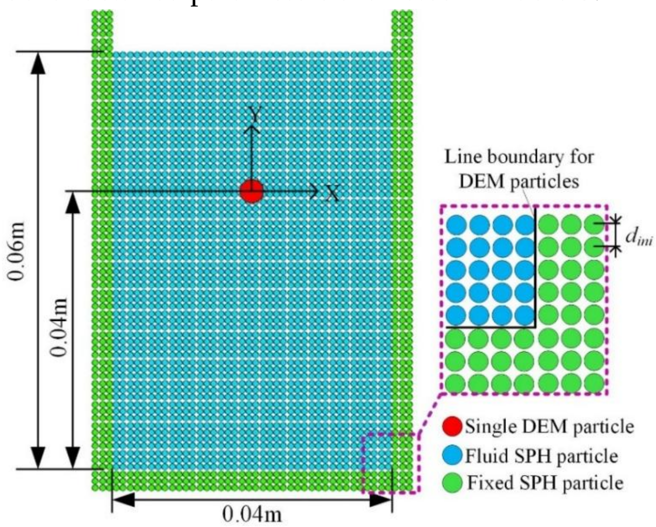

Figure 4. SPH-DEM Coupled model for single particle sedimentation

Table 3. Parameters for single particle sedimentation

Parameters	Value
Initial density for SPH particle, ρ_0	1.0×10^3kg/m^3
Viscocity for SPH particle, μ_f	1.0×10^{-2}Pa·s
Initial spacing for SPH particle, d_{ini}	1.0×10^{-3}m
Smoothing length for SPH-SPH, h	$1.25 \times d_{ini}$
Density for DEM particle, ρ_{dem}	1.25×10^3kg/m^3
Diameter for DEM particle, d	2.5×10^{-3}m
Coupling smoothing length for SPH-DEM, h_c	$2.5 \times d$
Time step, Δt	2.5×10^{-7}s

Boundary treatments for SPH and DEM are separately. For SPH particles, three layers of particles are fixed on the boundary to prevent fluid particles from penetrating. The velocity and acceleration of the boundary particles are fixed at zero, while other parameters (initial density, pressure, etc.) evolve through the kernel function as fluid particles do. A line boundary for DEM is placed at the boundary of water area, as shown in Fig.4. When the DEM particle's centroid is within the radius (radius of DEM particle) from the boundary. The particle is subjected to spring and damping forces from normal and tangential directions, as mentioned in Sec.3.2.

The DEM particle is released at t = 0s, moves along the negative Y direction under the action of gravity and coupling force, and finally stops at the bottom boundary. Fig.5 shows the time history of the DEM particle's velocity in Y direction. The simulation results are compared with the data in Reference [23]. The two processes of sedimentation are largely the same.

There are 3 different places. The first place is found at 0＜t＜0.20s when the particle accelerates down, which is caused by the drag force term $\boldsymbol{f}_d$ (Eq.(27)). Drag force increases with the relative speed between fluid and particle, so the acceleration is not a linear process. The second place occurs at 0.60＜t＜0.74s. When the DEM particle approaching the bottom boundary, the local fluid pressure at the bottom increases, resulting in the hydrodynamic force increase (Eq.(25)), which causes the particle to decelerate. The third place is at t = 0.74s when the particle contacts the bottom boundary. The particle rebounds by the contact force of spring-dashpot model, and finally stops at the bottom boundary. The results show that the coupled model can simulate the free movement of DEM particles in fluid phase.

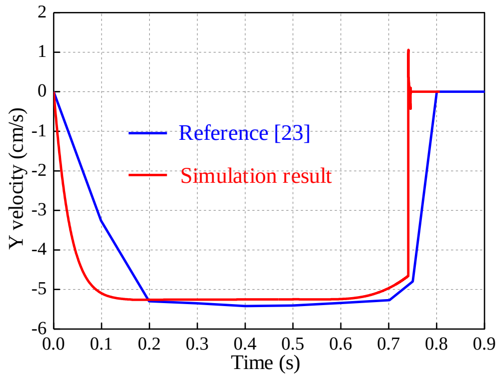

Figure 5. Time history of the velocity in Y direction

4.3 Case 2: high speed water-jet flow containing a single circular abrasive

The second case investigates the erosion process of solid phase by high speed water-jet impact. The computational domain is shown in Fig.6. The 2D numerical model is simplified, and the water-jet contains only one circular abrasive. The OFHC copper is set as the solid phase material with a size of 2.40×8.04mm. The water-jet diameter (d_{jet}) is 1.02mm, impacts the solid vertically at a speed of 200m/s. Water-jet SPH particles enter computational domain periodically from the inlet, and disappear at the outlet on both sides. These measures keep the particle number within a certain range and improve the computational efficiency.

Two types of rigid abrasive model are compared in this section. For Type 1 model, the circular abrasive is modeled by a single DEM particle. In Type 2 model, the abrasive is discretized with a series of SPH particles, as shown in Fig.6. The density and pressure evolution between abrasive SPH particles and water-jet particles are carried out by the kernel function with the smooth length h, and the contact force model for solid-abrasive interaction is the same as Eq.(23). Other details of Type 2 model are discussed in our earlier research [8]. The parameters for the single water-jet impact are listed in Table 5.

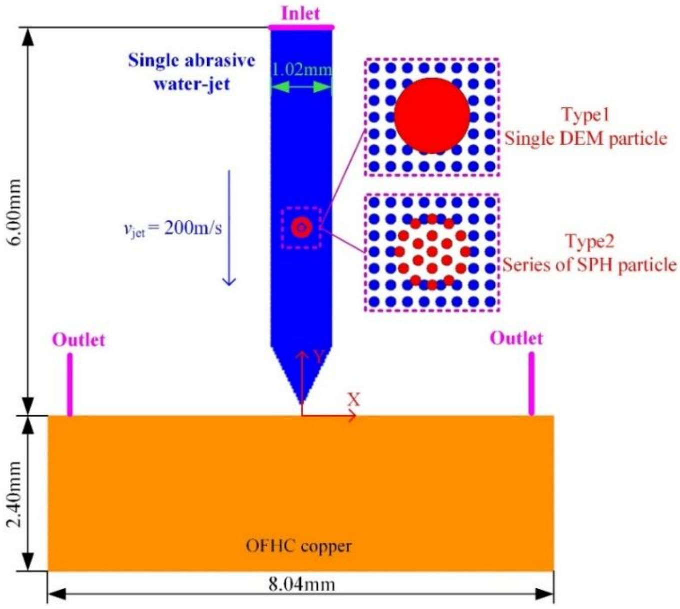

Figure 6. Single abrasive water-jet impact using 2 types of abrasive model

Table 5. Parameters for single abrasive water-jet impact

Parameters	Value
Initial density for water-jet SPH particle, ρ_0	1.0×10^3kg/m^3
Viscocity for water-jet SPH particle, μ_f	1.0×10^{-3}Pa·s
Initial spacing for SPH particle, d_{ini}	0.06mm
Smoothing length for SPH-SPH, h	$1.25 \times d_{ini}$
Density for circular abrasive, ρ_{ab}	7.8×10^3kg/m^3
Diameter for circular abrasive, d_{ab}	0.24mm
Coupling smoothing length for SPH-DEM, h_c	$2.0 \times d$
Time step, Δt	2.0×10^{-9}s

The simulation is conducted on a 16-core PC (E5-2667,3.20GHz), running about 6,0000 time steps with a corresponding physical time of 120μs. Fig.7 shows the evolution of the single abrasive water-jet impact. Type 1 single DEM particle model is shown in Fig.7(a~d), and Type 2 SPH particle model is shown in Fig.7(e~h). In these two models, the initial velocity of the abrasive is 200m/s. Under the action of fluid-abrasive interaction force, the abrasive impacts the solid SPH particles at a velocity of 170m/s at t = 30μs, finally flows to the side at t = 120μs.

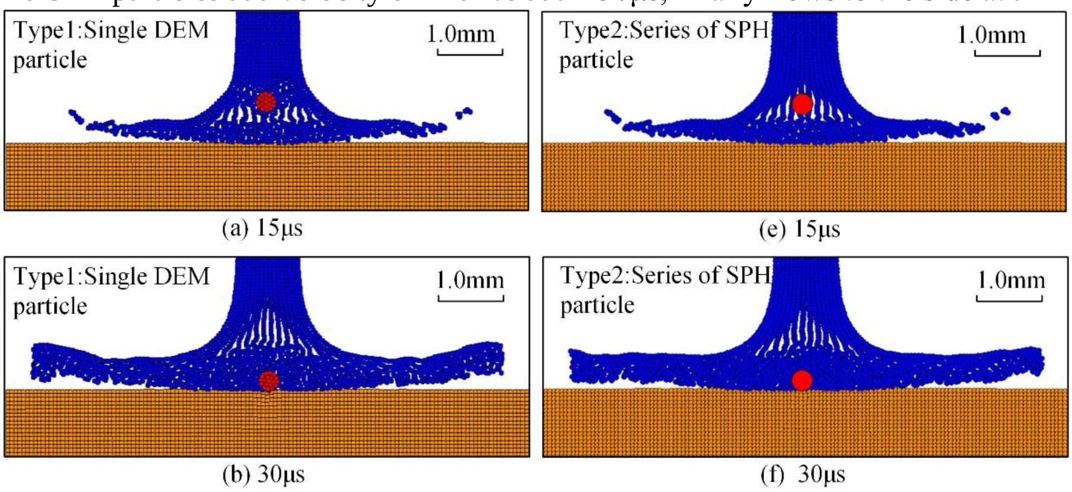

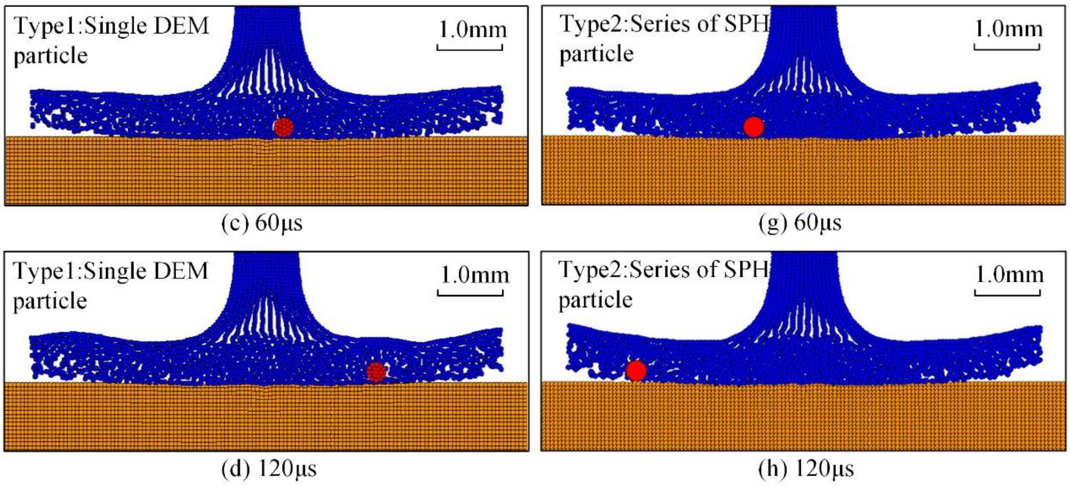

Figure 7. Evolution of single abrasive water-jet impact using 2 types of abrasive model

Surface morphology of OFHC copper by water-jet impact at t = 120μs is shown in Fig.8. The single abrasive impact solid at the center, causing plastic deformation on the surface, and leaving a small crater. The plastic strain distribution in both two types is basically the same, and maximum plastic strain is about 0.13. It can be concluded from Fig.7 and Fig.8 that the simulation results of the newly proposed coupled SPH-DEM model (Type 1) for single abrasive water-jet impact are consistent with the fully resolved SPH model (Type 2) in our previous study [8]. The main difference is the computation time. For the coupled SPH-DEM model, it takes about 840s to run 6,0000 time steps. While for the fully SPH model, the computation time cost is 894s. The proposed model saves 6% of computation time for the simulation of single abrasive water-jet impact.

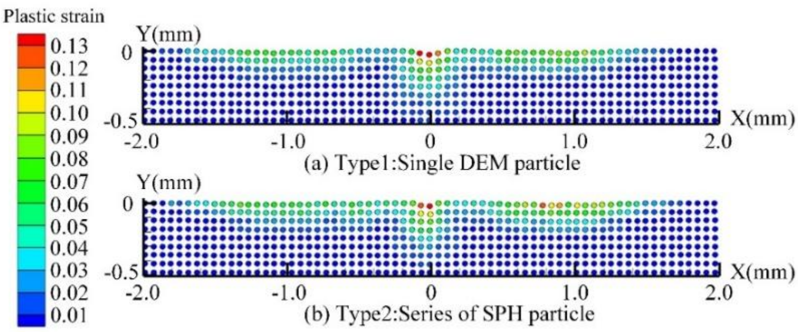

Figure 8. Surface morphology of OFHC copper at *t* = 120μs

For the meshfree particle method, the field variables of the particles (such as density, acceleration, stress, etc.) are calculated in pairs and accumulated. The most time-consuming part of the calculation is the neighborhood particle pair search. The link-list search method is adopted in this study. The information of two particles that are within 2 times the smoothing length is stored in memory in pairs for subsequent calculations. Obviously, the greater the number of particle pairs, the greater the amount of computation during the particle search, and the more time-consuming the computation will be. The number of particle pairs in two types (Niac1 for Type 1, and Niac2 for Type 2) are counted. Subtract these two numbers, as shown in Fig.9. Most of the time steps during the simulation, the Niac2−Niac1 value is greater than 0, which indicates that the coupled SPH-DEM model (Type 1) has fewer number of particle pairs. This may be the main reason for the less computation time cost of Type 1 model.

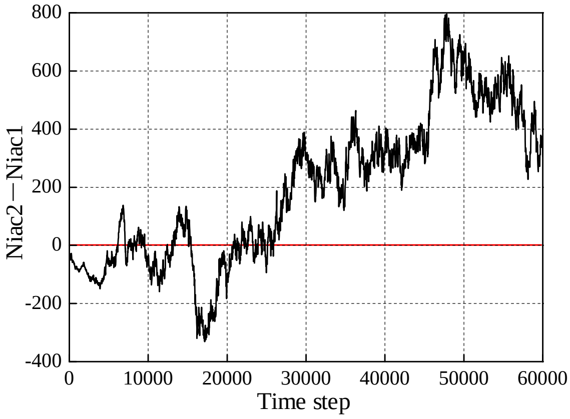

Figure 9. Difference of particle pair number in two types

It should be emphasized that the abrasive water-jet impact simulation in this study contains only one abrasive. If the water-jet contains multiple abrasives, the value of Niac2－Niac1 will be further increased, and the advantage of the coupled SPH-DEM model in less computation time cost will be more obvious, which will be involved in our further study.

5 Conclusions

In this study, a coupled SPH-DEM numerical model for AWJ impact simulation is proposed. The fluid and solid phases are discretized with a series of SPH particles, and the abrasive is modeled by a single DEM particle. Two numerical cases are carried out with the new model. The simulation results of single particle sedimentation are basically consistent with the reference. Compared with the fully resolved SPH model in our earlier research, the coupled model has less computation and higher numerical efficiency in single abrasive water-jet impact simulation. We believe that it has better effect in dealing with multiple abrasive water-jet impact. The present SPH-DEM model can reasonably describe the features of fluid–particle-solid coupling under free surface flow conditions.

References

[1] Canelas R B, Crespo A, JM Domínguez, et al. SPH–DCDEM model for arbitrary geometries in free surface solid–fluid flows[J]. Computer Physics Communications, 2016:131-140.

[2] Liu H T. Waterjet technology for machining fine features pertaining to micromachining[J]. Journal of Manufacturing Processes, 2010, 12(1):8-18.

[3] Tirumala D, Gajjela R, Das R. ANN and RSM approach for modelling and multi objective optimization of abrasive water jet machining process[J]. Decision Science Letters, 2018, 7(4): 535-548.

[4] Nyaboro J, Ahmed M, El-Hofy H, et al. Experimental and numerical investigation of the abrasive waterjet machining of aluminum-7075-T6 for aerospace applications[J]. Advances in Manufacturing, 2021, 9(2): 286-303.

[5] Kurnenkov A , Shurigin A , Glebov V . Investigation of the process of abrasive waterjet cutting of steels based on numerical simulation[J]. MATEC Web of Conferences, 2019, 298(2):00103.

[6] Dong X W, Li Z L, Jiang C , et al. Smoothed particle hydrodynamics (SPH) simulation of impinging jet flows containing abrasive rigid bodies[J]. Computational Particle Mechanics, 2019, 6(3): 479-501.

[7] Feng L, Liu G R, Li Z L, et al. Study on the effects of abrasive particle shape on the cutting performance of Ti-6Al-4V materials based on the SPH method[J]. The International Journal of Advanced Manufacturing Technology, 2019, 101(9): 3167-3182.

[8] Yu R, Dong X, Du M, et al. Improved smoothed particle hydrodynamics (SPH) model for simulation of abrasive water-jet (AWJ)[J]. International Journal of Computational Methods, 2022: 2143002.
[9] Takaffoli M, Papini M. Material deformation and removal due to single particle impacts on ductile materials using smoothed particle hydrodynamics[J]. Wear, 2012, 274: 50-59.
[10] Mao Z, Liu G R, Dong X W. A comprehensive study on the parameters setting in smoothed particle hydrodynamics (SPH) method applied to hydrodynamics problems[J]. Computers and Geotechnics, 2017, 92: 77-95.
[11] Liu G R, Liu M B. Smoothed particle hydrodynamics: a meshfree particle method[M]. World scientific, 2003.
[12] Monaghan J J, Lattanzio J C. A refined particle method for astrophysical problems[J]. Astronomy and astrophysics, 1985, 149: 135-143.
[13] T.B. Anderson, R. Jackson, Fluid mechanical description of fluidized beds. Equations of motion, Industrial and Engineering Chemistry Fundamentals 6(1967) 527–539.
[14] He Y, Bayly A E, Hassanpour A, et al. A GPU-based coupled SPH-DEM method for particle-fluid flow with free surfaces[J]. Powder technology, 2018, 338: 548-562.
[15] E.Y.M. Lo, S. Shao, Simulation of near-shore solitary wave mechanics by an incompressible SPH method, Applied Ocean Research 24 (2002) 275–286.
[16] Liu X H, Liu S Y, Ji H F. Numerical research on rock breaking performance of water jet based on SPH[J]. Powder Technology, 2015:181-192.
[17] Johnson G R, Cook W H. Fracture characteristics of three metals subjected to various strains, strain rates, temperatures and pressures[J]. Engineering fracture mechanics, 1985, 21(1): 31-48.
[18] Randles P W, Libersky L D. Smoothed particle hydrodynamics: some recent improvements and applications[J]. Computer methods in applied mechanics and engineering, 1996, 139(1-4): 375-408.
[19] Cundall PA, Strack ODL. A discrete numerical model for granular assemblies. Geotechnique 1979;29:47–65
[20] Norouzi H R, Zarghami R, Sotudeh-Gharebagh R, et al. Coupled CFD-DEM modeling: formulation, implementation and application to multiphase flows[M]. John Wiley & Sons, 2016.
[21] Campbell J, Vignjevic R, Libersky L. A contact algorithm for smoothed particle hydrodynamics[J]. Computer methods in applied mechanics and engineering, 2000, 184(1): 49-65.
[22] Anderson T B, Jackson R. Fluid mechanical description of fluidized beds. Equations of motion[J]. Industrial & Engineering Chemistry Fundamentals, 1967, 6(4): 527-539.
[23] Wu K, Yang D, Wright N, et al. An integrated particle model for fluid–particle–structure interaction problems with free-surface flow and structural failure[J]. Journal of fluids and structures, 2018, 76: 166-184.